ARTICLES
PUBLISHED ONLINE: 24 APRIL 2011 | DOI: 10.1038/NPHOTON.2011.49
nature photonics

Coherent sampling of active mode-locked terahertz quantum cascade lasers and frequency synthesis

Stefano Barbieri[1]*, Marco Ravaro[1], Pierre Gellie[1], Giorgio Santarelli[2], Christophe Manquest[1], Carlo Sirtori[1], Suraj P. Khanna[3], Edmund H. Linfield[3] and A. Giles Davies[3]

Terahertz quantum cascade lasers are compact, electrically pumped semiconductor laser sources that are capable of delivering tens of milliwatts of power in continuous wave. Here, we demonstrate that these devices can be operated in a regime of active mode-locking by modulating their bias current with a radiofrequency synthesizer. Detection of the emitted pulse train is made possible by phase-locking the quantum cascade laser repetition rate and carrier frequency to a harmonic of the repetition rate of a mode-locked femtosecond fibre laser. This technique allows coherent sampling of the terahertz electric field, showing that the terahertz pulses are transform-limited. In addition, our technique allows control of the carrier-envelope phase shift of the quantum cascade laser.

Quantum cascade lasers (QCLs) are unipolar semiconductor lasers based on electronic intersub-band transitions in the conduction band of multilayered heterostructures[1]. In contrast to interband diode lasers, in which the lifetime of the electrons populating the upper laser state is determined by electron–hole recombination, the electron lifetime in QCLs is dominated by non-radiative phenomena, and in particular optical–phonon scattering. This leads to fast relaxation times on a picosecond timescale, a characteristic that has an important effect on the dynamical properties of this family of devices[2]. In particular, modulation bandwidths of up to several tens of gigahertz have been demonstrated, which have recently been exploited to show that the frequency separation, or roundtrip frequency, between the longitudinal modes of multimode terahertz frequency QCLs[3–7] can be stabilized using an external radiofrequency (RF) synthesizer[8–11]. Under these conditions, the laser is expected to operate in a regime of active mode-locking, producing a train of short pulses. However, the lack of suitable detection techniques in the terahertz range has so far prevented the measurement of these pulses.

Difficulty in demonstrating QCL mode-locking has previously been encountered at mid-infrared (mid-IR) frequencies, and arises in part from the inefficiency of second-order autocorrelation techniques in the mid-IR (and terahertz) ranges, therefore hindering measurement of the emitted pulse train. The first reports of passive and active mode-locking of mid-IR QCLs[12,13] were later identified as coherent dynamic instabilities resulting from the fast gain recovery time (∼1 ps) preventing the formation of stable mode-locked pulses[14,15]. Recently, however, mode-locking of a QCL operating at 6.3 μm has been demonstrated using second-order autocorrelation with a two-photon quantum-well detector[16]. In this case, a specific active region had to be designed to increase the non-radiative upper-state lifetime to a few tens of picoseconds. Compared to mid-IR QCLs, terahertz QCLs based on bound-to-continuum active regions generally have longer non-radiative relaxation times of the upper laser state (∼5–10 ps) as a result of the laser transition energy lying below the optical phonon energy[17–19]. This probably plays a significant role in allowing us to demonstrate the results presented here.

In this Article, we show that terahertz QCLs can be operated in a regime of active mode-locking. The measurement proof of mode-locking operation is obtained by sampling the electric field amplitude emitted by the QCL using a mode-locked femtosecond laser. Mode-locked femtosecond lasers are established sources for probing fast transient phenomena, with pump–probe experiments using two mode-locked femtosecond lasers with slightly different repetition rates becoming widespread[20,21]. In these experiments, the time delay between the pump and the probe laser pulses is automatically scanned at the difference frequency of the repetition rates. This technique, known as asynchronous optical sampling, has recently been applied in the terahertz frequency range to probe broadband terahertz pulses generated with nonlinear optics[22–25]. In a broader context, over the past decade, pairs of femtosecond lasers have been used to demonstrate coherent optical pulse synthesis[26], and incoherent and coherent multiheterodyne spectroscopy in the near-IR and mid-IR ranges[27,28].

In our work, we use a commercial mode-locked erbium-doped femtosecond laser emitting at 1.55 μm (193 THz), for the asynchronous sampling of a mode-locked QCL emitting at 2.5 THz (ref. 7). Mode-locking of the QCL is obtained by direct modulation of its bias current close to the laser roundtrip frequency[11]. Asynchronous sampling is made possible by phase-locking the QCL source to the femtosecond laser; that is, the pulse repetition rate of the QCL at ∼13.3 GHz and its carrier frequency at 2.5 THz are simultaneously phase-locked to a harmonic of the repetition rate of the femtosecond laser comb at 96.5 MHz (refs 11,29). There are two advantages to this technique. First, it enables coherent sampling of the terahertz QCL waveform over virtually unlimited timescales, allowing us to prove unambiguously that the device is operating in a regime of active mode-locking, and is generating ∼10-ps-wide, transform-limited pulses. Second, it gives control of

[1]Laboratoire Matériaux et Phénomènes Quantiques, Université Paris 7 and CNRS UMR 7162, 10 rue A. Domont et L. Duquet, 75205 Paris, France, [2]LNE-SYRTE, CNRS, UPMC, Observatoire de Paris, 61 avenue de l'Observatoire, 75014 Paris, France, [3]School of Electronic and Electrical Engineering, University of Leeds, Leeds LS2 9JT, United Kingdom. *e-mail: stefano.barbieri@univ-paris-diderot.fr

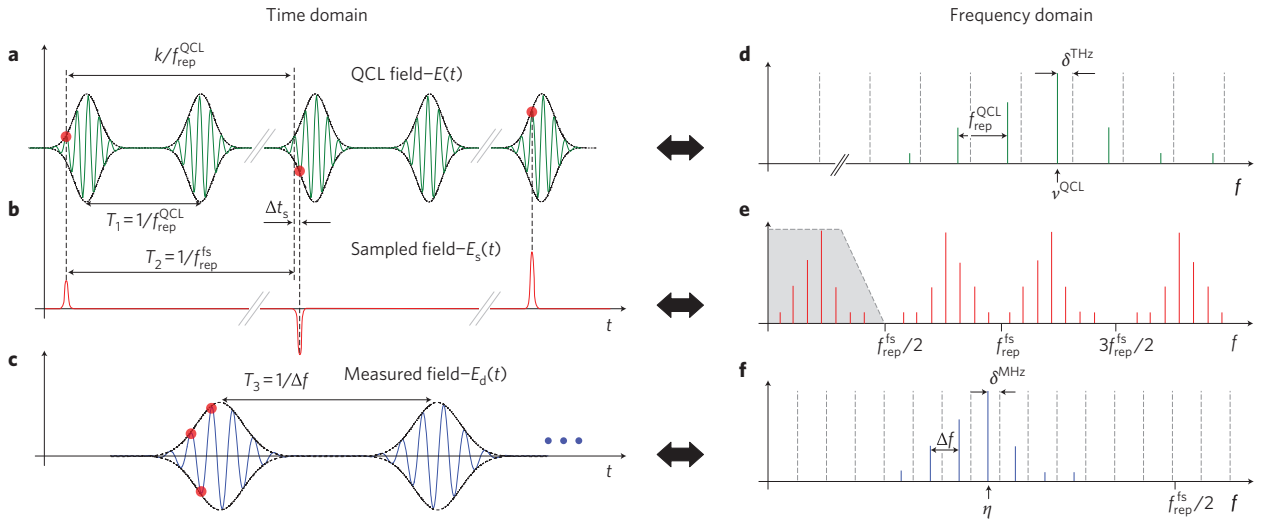

Figure 1 | Schematic diagram showing sampling of the terahertz QCL emission by a femtosecond laser in the time domain (left) and frequency domain (right). a, Original terahertz pulse train electric field amplitude (green curve). The black curve represents the pulse envelope and the red dots indicate the sampled points. **d**, Fourier transform of the original pulse train. **b**, Sampled terahertz pulse train by the femtosecond laser pulse train (see equation (2)). The sampling time step is given by $\Delta t_s = 1/f_{rep}^{fs} - k/f_{rep}^{QCL}$, where $k = \mathrm{int}(f_{rep}^{QCL}/f_{rep}^{fs})$. In the example in the figure Δt_s is equal to 0.5 THz cycles. One in every k QCL pulses is sampled by the femtosecond laser. **e**, Fourier transform of the sampled terahertz pulse train. Following equation (4), the spectrum is composed of replicas of the Fourier transform of $E_d(t)$, centred at $n \times f_{rep}^{fs}$, where n is an integer. The shaded area indicates the modes selected by low-pass filtering (see text). **c**, Down-converted terahertz pulse train after the low-pass filtering process. The repetition rate is $\Delta f = f_{rep}^{QCL} - k \times f_{rep}^{fs}$. **f**, Fourier transform of the down-converted terahertz pulse train. The new carrier frequency is $\eta = \nu_{QCL} - r \times f_{rep}^{fs}$, where $r = \mathrm{int}\,(\nu_{QCL}/f_{rep}^{fs})$. In **d** and **f**, the vertical dashed lines are integer multiples of f_{rep}^{QCL} and Δf respectively, and δ^{THz} and δ^{MHz} indicate the corresponding carrier-envelope frequency offsets[31] of the original terahertz QCL and of the down-converted comb. Note that, in general, these will be different, resulting in different pulse-to-pulse phase shifts.

the QCL carrier-envelope phase shift, and allows terahertz frequency synthesis[30,31].

Results

Detection technique. In contrast to traditional experiments that involve two femtosecond lasers with slightly different repetition rates[20–25], in this work the repetition rates of the mode-locked QCL and femtosecond laser differ by more than two orders of magnitude (13 GHz and 100 MHz). To derive an expression for the sampled waveform emitted by the QCL, from now on we will assume that the device is mode-locking, and is generating a pulse train with a repetition rate f_{rep}^{QCL}. The amplitude $E(t)$ of the emitted electric field can be written as the sum of the electric field of each of the QCL longitudinal modes. The frequency of each mode can be expressed in terms of its difference from the frequency of one of the modes, ν_{QCL}, which will be termed the carrier frequency (Fig. 1a). Because the separation between the modes is given by f_{rep}^{QCL}, we can express the sum as

$$E(t) = \exp(i \cdot 2\pi\nu_{QCL} \cdot t) \times \sum_{m=-q}^{m=+p} E_m \exp[i \cdot (2\pi m f_{rep}^{QCL} \cdot t + \phi_m)] + cc. \quad (1)$$

where there are q/p longitudinal modes with frequencies below/above ν_{QCL}, respectively, and E_m and ϕ_m are their amplitudes and phases, respectively. The total number of modes is $M = q + p$. Now, assume that the QCL electric field can be sampled by the femtosecond laser using an appropriate technique (see next section). Then the sampled field, $E_s(t)$, can be expressed as

$$E_s(t) = E(t) \sum_{n=-\infty}^{n=+\infty} \delta\left(t - \frac{n}{f_{rep}^{fs}}\right) \quad (2)$$

where f_{rep}^{fs} is the pulse repetition rate (96 MHz) of the femtosecond laser (Fig. 1b). For the purpose of calculating the sampled field, the assumption that the pulse train emitted by the femtosecond laser can be approximated by an equally spaced series of δ-functions is valid if the femtosecond pulse duration, $\tau_p^{fs} \approx 100$ fs, is shorter than the period of the carrier wave, or

$$\tau_p^{fs} < 1/\nu_{QCL} \quad (3)$$

In this case, $\tau_p^{fs} \approx 100$ fs and $1/\nu_{QCL} \approx 400$ fs, so the condition is satisfied[29]. Note that, because $f_{rep}^{fs} \ll f_{rep}^{QCL}$, $E(t)$ is heavily undersampled. Now, by combining equations (1) and (2) (see Methods for a detailed derivation), we obtain

$$E_s(t) = \left[\exp(i \cdot 2\pi\eta \cdot t) \times \sum_{m=-q}^{m=+p} E_m \exp[i \cdot (2\pi m\Delta f \cdot t + \phi_m)]\right] \times \sum_{n=-\infty}^{n=+\infty} \delta\left(t - \frac{n}{f_{rep}^{fs}}\right) + cc. = E_d(t) \times \sum_{n=-\infty}^{n=+\infty} \delta\left(t - \frac{n}{f_{rep}^{fs}}\right) \quad (4)$$

Here $\eta = \nu_{QCL} - r \times f_{rep}^{fs}$ and $\Delta f = f_{rep}^{QCL} - k \times f_{rep}^{fs}$, with $r = \mathrm{int}\,(\nu_{QCL}/f_{rep}^{fs})$ and $k = \mathrm{int}\,(f_{rep}^{QCL}/f_{rep}^{fs})$. From a comparison with equation (1), it can be seen that $E_d(t)$ is a replica of the terahertz QCL waveform, where the original repetition rate and carrier frequency, f_{rep}^{QCL} and ν_{QCL}, are replaced by Δf and η, given respectively by the difference between f_{rep}^{QCL} and ν_{QCL} and their closest harmonics of f_{rep}^{fs}. As such, $E_d(t)$ represents the lowest frequency waveform that gives $E_s(t)$, when sampled at the same rate as $E(t)$. Now, because the new repetition rate $\Delta f < f_{rep}^{fs}$, $E_d(t)$, in contrast to $E(t)$, does not suffer from undersampling (only one in every k QCL pulses is sampled by the femtosecond laser) and can therefore be fully retrieved from $E_s(t)$. In more rigorous terms, according to the

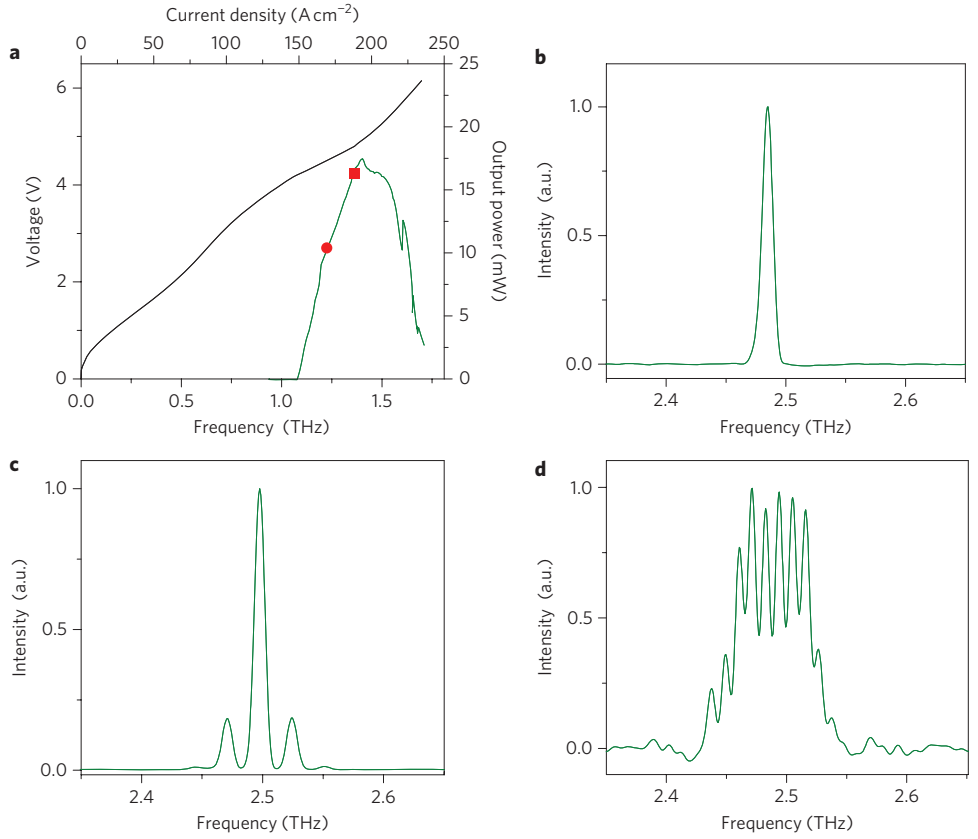

Figure 2 | Electrical and optical characteristics of the terahertz QCL operated in continuous wave at a heat-sink temperature of 20 K. a, Voltage/current (black line) and output power/current (green line) characteristics. **b**, Emission spectrum measured at a drive current of 1.24 A (red circle in **a**). The spectrum is single mode. The linewidth is limited by the 7.5 GHz resolution of the FTIR spectrometer. **c**, Emission spectrum measured at a drive current of 1.35 A (red square in **a**). The separation between the longitudinal modes is ~26.6 GHz (equal to twice f_{rep}^{QCL}). **d**, Emission spectrum measured at a drive current of 1.35 A. In this case, the current of the QCL was modulated by RF-1 with +10 dBm of RF power at a frequency of 13.315 GHz (see set-up of Fig. 3).

Nyquist theorem, a full retrieval is possible provided that twice the spectral bandwidth of $E_d(t)$ is smaller than the sampling rate (that is, provided that $M \times \Delta f < f_{rep}^{fs}/2$). If this is the case, then $E_d(t)$ can be obtained by filtering $E_s(t)$ with a low-pass filter of bandwidth $f_{rep}^{fs}/2$. (Note that equation (4) can be applied to the asynchronous sampling used in terahertz time-domain spectroscopy, as in refs 22–25. In this case, due to the nonlinear generation of the terahertz pulse, the carrier frequency is an integer multiple of the repetition rate of one femtosecond laser; that is, $\eta = 0$. Also, the sampling process can be seen as a modulation of the femtosecond laser pulse train by the QCL electric field (see equation (2) and ref. 29). In such a picture the spectrum of Fig. 1f can be seen as the result of the heterodyne beat between the lines of the femtosecond laser spectrum and those of its M sidebands generated by the terahertz modulations at $(\nu_{QCL} + m \times f_{rep}^{QCL})$, with $-q \leq m \leq \pm p$).

The entire sampling process in the time and frequency domains is schematically illustrated in Fig. 1a–c, which shows the original pulse train at a repetition rate f_{rep}^{QCL} (equation (1)), the sampled trace at f_{rep}^{fs} (equations (2) and (4)) and $E_d(t)$, together with their Fourier transforms. An important point to note (Fig. 1a,b and its caption) is that the effective time step between two sampled points is given by $\Delta t_s = \Delta f/(f_{rep}^{fs} \cdot f_{rep}^{QCL})$ (ref. 25). This determines the time resolution, which can in principle be reduced at will by reducing Δf until Δt_s reaches τ_p^{fs}, which sets the ultimate resolution. Equation (3) ensures that in this case the terahertz carrier is properly sampled. Finally, it is worth noting that, in general, the terahertz and sampled spectra will not have the same carrier-envelope frequency offsets (δ^{THz} and δ^{MHz} in Fig. 1d,f). This is reflected by the sampled time trace having a relative carrier-envelope phase that is different from that of the original terahertz waveform (Fig. 1a,c)[31].

Experimentally, the challenge of this work consists in making the sampling of the terahertz QCL coherent. This can be achieved by stabilizing η and Δf in equation (4), that is, from their expressions given above, by stabilizing ν_{QCL} and f_{rep}^{QCL} relative to f_{rep}^{fs}. In this case, the time jitter between the QCL waveform and the femtosecond laser repetition rate is eliminated, guaranteeing that during the acquisition time the sampled signal accumulates coherently, leading to very high signal-to-noise ratios.

Experimental set-up and phase-locking. Figure 2 presents the electrical and optical characteristics of the QCL used in this work. The emission spectra were collected with a Fourier transform infrared (FTIR) spectrometer with a spectral resolution of 7.5 GHz. The device is a 3-mm-long, 240-μm-wide ridge, embedded in a single plasmon waveguide[7]. The QCL was mounted on the cold head of a continuous-flow helium cryostat, and kept at a stabilized temperature of 20 K. At a low current (1.24 A, Fig. 2b), the emission is single mode, centred close to 2.5 THz. At higher currents (1.35 A, Fig. 2c), we observe the appearance of three longitudinal modes, separated by ~26.6 GHz, that is, twice f_{rep}^{QCL} (ref. 11). The maximum emitted power is ~17 mW (Fig. 2a), and was measured with a calibrated pyroelectric detector.

The experimental arrangement for the phase-locking of the QCL to the femtosecond laser is shown in Fig. 3. We used three synthesizers, labelled RF-1, RF-2 and RF-3, sharing the 10 MHz reference of RF-1. RF-1 was used, with the help of a bias-T, to modulate the bias current of the QCL at a frequency f_{RF1}, close to

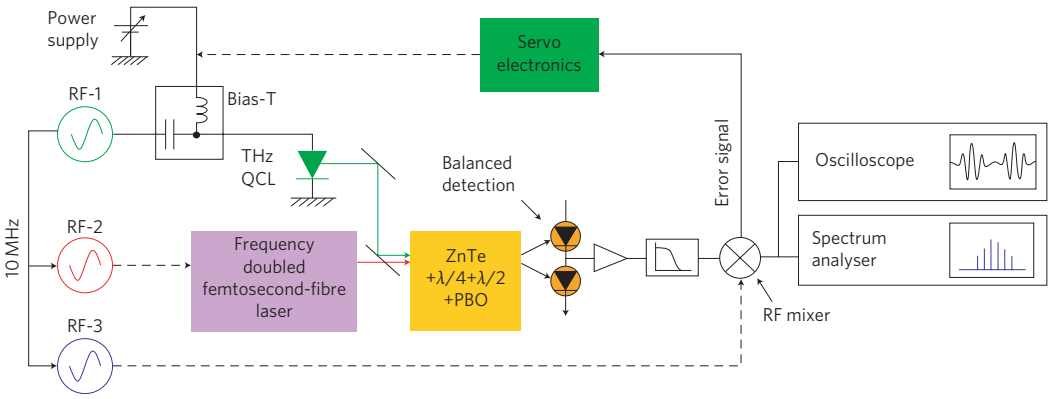

Figure 3 | Experimental set-up. The terahertz QCL is driven in continuous wave with a commercial power supply. Synthesizer RF-1 is connected to the QCL through a bias-T with a bandwidth of 15 GHz. Synthesizer RF-2 is used to control the repetition rate of the femtosecond laser, $f_{rep}^{fs} = 96.513$ MHz. The frequency-doubled (775 nm) power output of the femtosecond laser (1,550 nm wavelength, 100 fs pulsewidth, 96 MHz repetition rate) is ~50 mW. The ZnTe crystal is 2 mm thick, and is followed by $\lambda/4$ and $\lambda/2$ waveplates, a polarizing beamsplitter (PBO), and a fast balanced photodetector (see Methods). The output of the balanced detector, after being amplified and filtered with a lowpass filter of ~50 MHz bandwidth, is phase-compared using an RF mixer to the signal generated by synthesizer RF-3. RF-1, RF-2 and RF-3 share a common 10 MHz clock. The dashed arrows indicate the active controls of the QCL carrier frequency and of the fs-laser repetition rate.

the free-running f_{rep}^{QCL}. Figure 2d shows an emission spectrum obtained by driving the QCL at the same current as in Fig. 2c, but with RF-1 delivering +10 dBm of RF power at $f_{RF1} = 13.32$ GHz. As a result of the modulation, we observe the appearance of ~10 Fabry–Pérot (FP) modes above threshold, separated by f_{RF1}. As shown in ref. 11, for a given RF power, when the modulation frequency is sufficiently close to f_{rep}^{QCL} (to within ~100/200 MHz), the QCL becomes injection-locked; that is, $f_{RF1} = f_{rep}^{QCL}$.

The synthesizer RF-2 was used to phase-lock f_{rep}^{fs}. This was achieved using servo control electronics that fed back into a piezoelectric transducer and a stepper motor to control the femtosecond laser cavity length. The loop bandwidth was on the order of a few 100 Hz. Having RF-2 referenced to the 10 MHz clock of RF-1 ensured that f_{rep}^{QCL} was phase-locked to f_{rep}^{fs}, making Δf constant (see equation (4)).

To sample the terahertz QCL electric field, radiation from the frequency-doubled femtosecond laser and the QCL were simultaneously focused on a ZnTe-based electro-optic cell (Fig. 3; see Methods and ref. 29 for a detailed description). The sampled beam was subsequently detected using a fast balanced detection unit with a bandwidth of ~300 MHz, and filtered by a low-pass filter with a bandwidth of 50 MHz; that is, approximately equal to $f_{rep}^{fs}/2$ (Fig. 1e). This allowed the recovery of the down-converted terahertz QCL pulse train given by $E_d(t)$ in equation (4) (Fig. 1c). Figure 4a shows an example of a spectrum of $E_d(t)$ recorded with a spectrum analyser with resolution bandwidth (RBW) of 100 kHz, and a sweep time of 5.5 ms. Here, the QCL was kept at a temperature of 20 K, and driven in continuous wave at a current of 1.35 A. The device current was then modulated by RF-1, with an RF power of +10 dBm and a modulation frequency $f_{RF1} = 13.321794$ GHz. The frequency of RF-2 was set at $f_{RF2} = f_{rep}^{fs} = 96.513$ MHz. Nine narrow lines can be clearly observed in the spectrum. As predicted by equation (4), they are separated by $\Delta f = f_{RF1} - 138 \times f_{rep}^{fs} = 3$ MHz, and correspond to the down-converted longitudinal terahertz modes of the QCL spectrum at frequencies $\eta + m \times \Delta f$ (see equation (4) and Fig. 1f). Their instantaneous linewidth on a sweep time of ~5 ms is of the order of 100 kHz. Figure 4b shows the same spectrum as Fig. 4a, but acquired with the Max–Hold function of the spectrum analyser switched ON for ~1 s. The lines are significantly broadened as a consequence of the fact that ν_{QCL} is not phase-locked to f_{rep}^{fs}, and is therefore subject to fluctuations due to thermal and current instabilities of the QCL[32–34]. As shown in equation (4), these

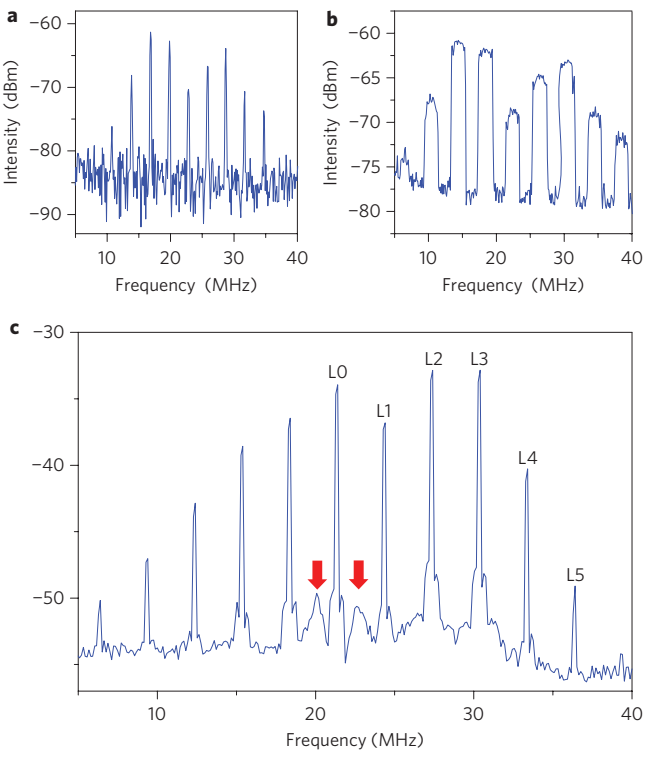

Figure 4 | RF spectra of the sampled THz waveform. a, Single-shot trace of the down-converted terahertz QCL spectrum recorded with a RBW of 100 kHz, and a sweep time of 5.5 ms. The QCL is driven at a current of 1.35 A (Fig. 2d) and is modulated with +10 dBm of RF power, and frequency $f_{RF1} = 13.321794$ GHz ⇒ $\Delta f = 3$ MHz is the frequency interval between the lines. In this spectrum, the loop that controls ν_{QCL} is left open. **b**, Spectrum collected with the Max-Hold function of the spectrum analyser switched ON for ~1 s. In this case, $f_{RF1} = 13.322794$ GHz ⇒ $\Delta f = 4$ MHz. As in **a**, the loop that controls ν_{QCL} is left open. **c**, Spectrum collected with a RBW of 100 kHz and 100 video averages. Here, $f_{RF1} = 13.315794$ GHz ⇒ $\Delta f = 3$ MHz. In this spectrum, $f_{RF3} = 21.3$ MHz, which allows phase-locking of the sixth line from the left (labelled L0) to f_{rep}^{fs}. The wings indicated by the red arrows on both sides of L0 show that the bandwidth of the phase-locked loop is ~1.5 MHz (ref. 29). Compared to panels **a** and **b**, the signal was amplified by a further 30 dB.

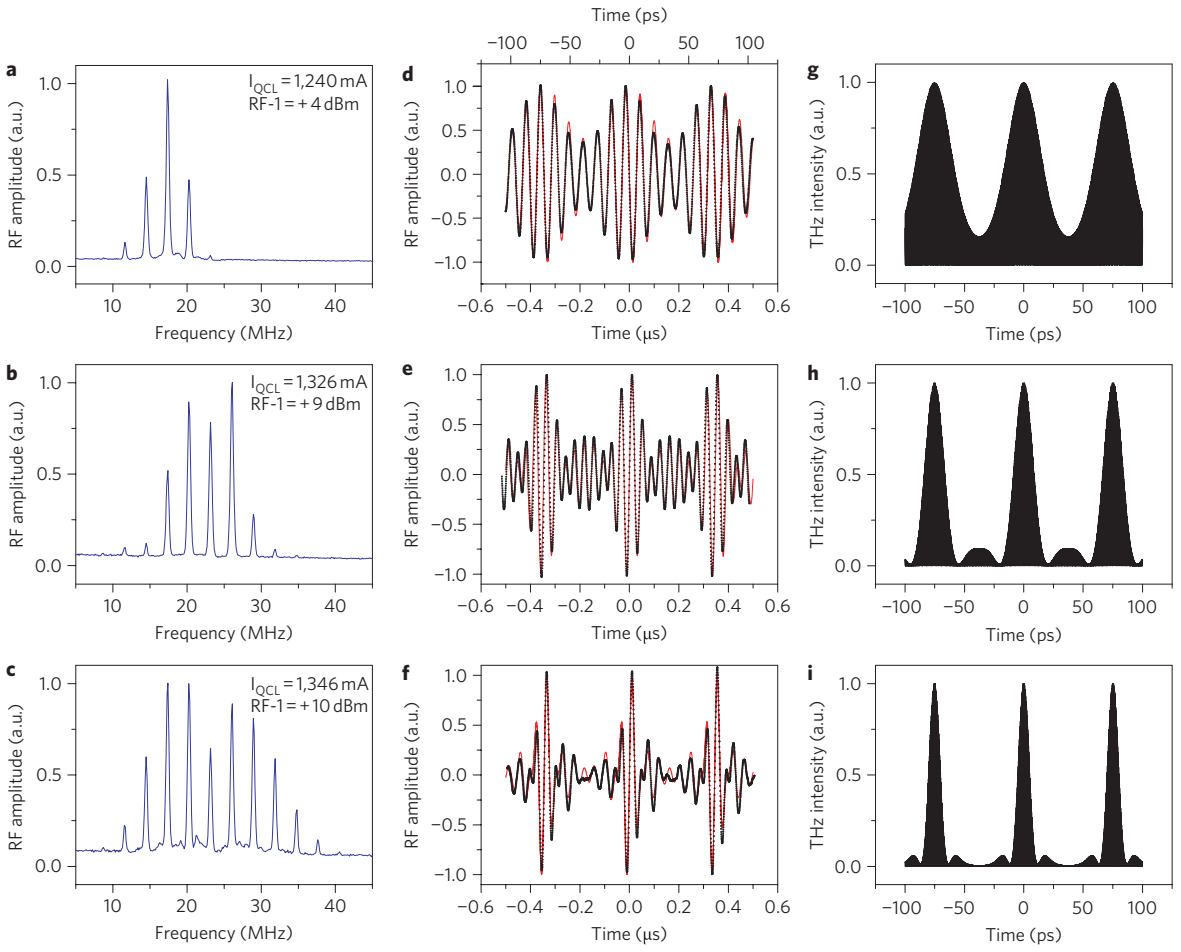

Figure 5 | Mode-locked operation of the terahertz QCL under simultaneous injection- and phase-locking for an increasing number of longitudinal modes. Left column: RF experimental spectra in linear scale with f_{rep}^{fs}= 96.513 MHz, f_{rep}^{QCL} = 13.315894 GHz and Δf = 2.9 MHz. Central column: corresponding experimental waveforms (dots), and calculated waveforms assuming (red lines) that all modes have equal phases ($\Delta\phi = 0$). The bottom axis shows the effective measured timescale on the oscilloscope (Fig. 1c). The top axis shows the original timescale (Fig. 1c) obtained by rescaling the measured timescale by the factor ($\Delta f/f_{rep}^{QCL}$). The sampling step is $\Delta t_s \approx 2.3$ ps, that is, equal to approximately six optical cycles at 2.5 THz. Note that all the measured pulses are identical. Indeed, the waveforms were obtained by setting $f_{RF3} = 7 \times \Delta f = 20.3$ MHz, so that $\eta = 0$, which gives a null carrier-envelope phase shift for the sampled terahertz pulse train (see equation (4), expression within brackets). Right column: computed pulse intensity in the terahertz range obtained from equation (1) with $\phi_m = 0$, $\forall m$, and using the measured values of E_m (Fig. 1c) and ν_{QCL} (2.5 THz; see Fig. 2). **a**,**d**,**g**, 1,240 mA drive current, +4 dBm RF power. **b**,**e**,**h**, 1,326 mA drive current, +9 dBm RF power. **c**,**f**,**i**, 1,346 mA drive current, +10 dBm RF power.

fluctuations are transferred to $\eta = \nu_{QCL} - f_{rep}^{fs} \times \text{int}\ (\nu_{QCL}/f_{rep}^{fs})$, resulting in rigid shifts of the terahertz comb lines. Indeed the latter are always separated by $\Delta f = 3$ MHz thanks to the phase-locking of f_{rep}^{QCL} to f_{rep}^{fs}. This is reflected by the fact that all lines of the spectrum of $E_d(t)$ of Fig. 4b have an identical width of ~2 MHz.

To complete the locking of the QCL to the femtosecond laser we need therefore to phase-lock ν_{QCL} to f_{rep}^{fs}. This is achieved using the technique described in ref. 29. Essentially, one of the lines of the spectrum of Fig. 2b, at frequency $(\eta + m \times \Delta f)$ (see equation (4)), is compared, using a RF mixer, to a reference signal generated by synthesizer RF-3, at f_{RF3}. As shown in Fig. 3, the error signal, oscillating at the difference frequency $(\eta + m \times \Delta f) - f_{RF3}$, is fed into fast phase-lock electronics and used to control a small fraction of the terahertz QCL bias current. Figure 4c shows the down-converted QCL spectrum obtained with the simultaneous phase-locking of f_{rep}^{QCL} and ν_{QCL} to f_{rep}^{fs}, and measured under the same conditions as for Fig. 4b. In this case, f_{RF3} was set to 21.3 MHz, which allows phase-locking the sixth line from the left of the spectrum (labelled L0). The positions of the wide wings on either side of this line (red arrows) indicate that the bandwidth of the phase-locked loop is ~1.5 MHz (ref. 29). Despite the Max–Hold function of the spectrum analyser being ON for several seconds, the width of all the lines is still only 100 kHz, showing the effect of the phase-coherent locking of the QCL to the femtosecond laser. Since the measured linewidth corresponds to the RBW of the measurement, the true linewidths are even narrower. A rigorous proof that all the lines of the spectrum of Fig. 4c are phase-locked with a sub-hertz linewidth can be found in Methods.

Active mode-locking of the terahertz QCL and frequency synthesis. Figure 5 shows three examples of phase-locked time-domain traces (middle column, black curves) for different RF-1 powers, and the corresponding RF spectra of $E_d(t)$ on a linear scale (left column). The time traces were recorded using an oscilloscope with a 100 MHz bandwidth (Fig. 3). The trace in Fig. 5d was obtained with the QCL driven at 1.24 A, and with RF-1 delivering +4 dBm of RF power. The time trace is composed of a fast component modulated by a slower envelope oscillating at $\Delta f = f_{RF1} - 138 \times f_{rep}^{fs} = 3$ MHz. As shown by the RF spectrum in Fig. 5a, the trace is generated by the QCL emitting on three longitudinal modes, and corresponds to the terahertz QCL mode-locked output being sampled by the femtosecond

laser with a time step $\Delta t_s = \Delta f/(f_{rep}^{fs} \cdot f_{rep}^{QCL}) \approx 2.3$ ps (the top horizontal axis in Fig. 5d shows the original timescale obtained by rescaling the measured timescale by the compression factor $\Delta f/f_{rep}^{QCL}$). The trace was collected with 1,000 averages, over a measuring time of a few seconds, corresponding to more than 10^{10} roundtrips of the terahertz QCL. As discussed previously, Δt_s could in principle be reduced by reducing Δf, therefore eliminating undersampling ($\Delta t_s \approx 2.3$ ps corresponds to approximately six optical cycles at 2.5 THz). However, in practice, we found that the frequency of the down-converted lines must be kept apart by approximately twice the servo bandwidth needed for the phase-lock of ν_{QCL} (of the order of 1.5 MHz, see Fig. 4c), otherwise the overlapping phase noise of each beat prevents locking[29]. This presently limits the minimum achievable Δf to ~3 MHz. Figure 5e,f shows two additional time traces, this time with the QCL being driven at higher currents and modulated with higher RF powers. At 1.346 A and with +10 dBm of RF power we were able to drive 10 longitudinal modes above threshold, producing mode-locked pulses with a duration of ~10 ps (Fig. 5c,f,i).

By setting $f_{RF1} = 13.318794$ MHz $= 138 \times f_{rep}^{fs}$, $\Delta f = 0$ and all lines of the down-converted spectrum are degenerate. In this special case we verified that it is still possible to simultaneously phase-lock the QCL modes. This implies that the values of ϕ_m in equation (1) have a monotonic and weak phase dispersion, with a maximum total phase-change of less than $\pi/2$. This type of phase dispersion is predicted by the nonlinear theory of actively mode-locked lasers, in the case of an inhomogeneously broadened gain curve, wider than the longitudinal mode separation[35]. This condition is fulfilled by the present laser, and by terahertz QCLs in general, for which the gain curve is at least several hundreds of gigahertz wide[36–38]. Here, in particular, given the small number of longitudinal modes, we expect the effect of phase-dispersion to be negligible. The red curves in the central column of Fig. 5 represent the calculated time traces obtained from the expression of $E_d(t)$ in equation (4), with the E_m values given by the measured line amplitudes (left column of Fig. 5) and with the $\phi_m = 0, \forall m$. The agreement with the measured time traces is remarkably good, indeed showing that the pulses emitted by the mode-locked QCL are not significantly influenced by phase dispersions; that is, they are transform-limited. A Fourier analysis of the waveform has confirmed this finding.

To remove the effect of undersampling, the right column of Fig. 5 shows the reconstructed pulse intensity ($\propto (E(t))^2$) in the terahertz range obtained from equation (1) with $\phi = 0, \forall m$, $\nu_{QCL} = 2.5$ THz (Fig. 2), and using the measured values of E_m. In the bottom trace the pulse width is ~10 ps. Note that the value of ν_{QCL} is determined by the spectra of Fig. 2, with a precision of 7.5 GHz, as given by the resolution of our Fourier transform spectrometer.

In other words, the carrier-envelope offset frequency of the terahertz pulse train is unknown. This is irrelevant in the present case because the pulses are composed of several tens of terahertz cycles (this is why the terahertz oscillations are not discernible in the plotted pulse intensities).

Discussion

We have directly observed active mode-locking of a terahertz QCL by coherent asynchronous sampling of the emitted waveform. Our technique is based on phase-locking of the actively mode-locked terahertz QCL to a harmonic of the repetition rate of a femtosecond fibre laser. This allows simultaneous control of the QCL carrier frequency and repetition rate, that is, of its carrier-envelope phase shift[31], and represents the first report of coherent optical sampling of a mode-locked laser. The sampling technique demonstrated in this Article can be applied generally to any laser, provided that one optical cycle of the emitted radiation is longer than the femtosecond-laser pulse width.

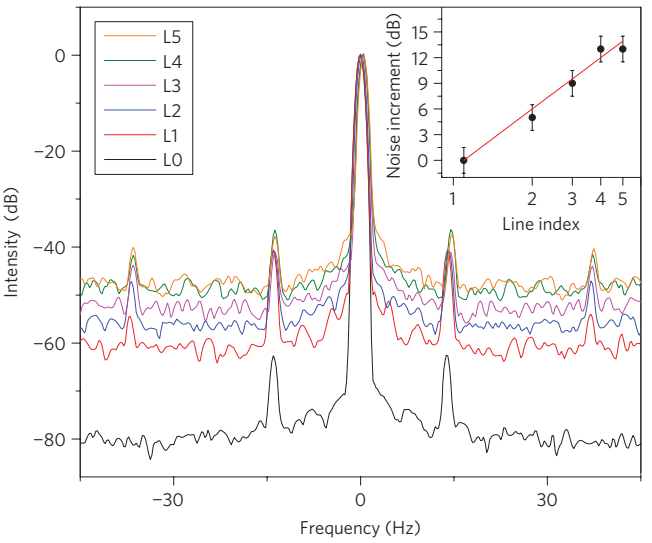

Figure 6 | Spectra of the phase-locked lines labeled L0 to L5 in Fig. 4c, measured with a RBW of 1 Hz, and 30 video averages. The frequency of each line was offset to zero, and its intensity normalized to 1 (0 dB). Inset: relative phase-noise increment from L1 as a function of line index, obtained from the spectra in the main figure at 30 Hz from the carrier frequency (black dots). The red line represents the expected noise increment, given by $10 \times \log(n^2)$, where n is the line index.

As well as providing a proof of principle that paves the way to the use of terahertz QCLs for the synthesis of pulses with high repetition rate and average power, our results prove unambiguously that these devices can be actively mode-locked to produce transform-limited pulses. As discussed in the introduction, mode-locking operation is more likely to occur in terahertz QCLs than in mid-IR devices. This is attributed to a longer non-radiative lifetime when the laser transition energy is below the optical phonon. To this end, the technique demonstrated in this work could be used as a tool for systematically studying the dynamics of mode-locked QCLs and also to help in elucidating the role played by the non-radiative lifetime in the process of pulse formation[14,15,39,40]. From a more technological point of view, exploiting the wide spectral gain of terahertz QCLs to produce shorter pulses is another interesting topic for future investigations. Indeed, in principle, it should be possible to significantly extend the bandwidth by at least several hundreds of gigahertz by appropriate design of the active region, and thus decrease the pulse duration towards ~1 ps (refs 39,41). Thanks to their high average power, such wideband terahertz QCLs, combined with the coherent detection demonstrated here, could become an alternative to present terahertz time-domain systems in spectroscopic and imaging applications[42].

Methods

Derivation of the sampled waveform. We begin with the expression of the electric field amplitude of the QCL:

$$E(t) = \exp(i \cdot 2\pi\nu_{QCL} \cdot t) \times \sum_{m=-q}^{m=+p} E_m \exp[i \cdot (2\pi m f_{rep}^{QCL} \cdot t + \phi_m)] + cc. \quad (1)$$

By expanding equation (2) in a Fourier series the sampled electric field can be expressed as

$$E_s(t) = E(t) \sum_{n=-\infty}^{n=+\infty} \delta\left(t - \frac{n}{f_{rep}^{fs}}\right) = E(t) \times f_{rep}^{fs} \sum_{n=-\infty}^{n=+\infty} \exp(i \cdot 2\pi n f_{rep}^{fs} \cdot t) \quad (5)$$

This equation implies that the bandwidth of the femtosecond laser is infinite (that is, the comb has an infinite number of lines). As explained in the main text, this is a good approximation if the femtosecond-laser bandwidth is larger than the carrier

frequency of $E(t)$ (that is, if $\tau_p^{fs} < 1/\nu_{QCL}$), which is the case in our experiment. From equations (1) and (5) we obtain

$$E_s(t) = \exp(i \cdot 2\pi\nu_{QCL} \cdot t) \times f_{rep}^{fs} \sum_{m=-q}^{m=+p} E_m \exp[i \cdot (2\pi m f_{rep}^{QCL} \cdot t + \phi_m)] \times \sum_{n=-\infty}^{n=+\infty} \exp(i \cdot 2\pi n f_{rep}^{fs} \cdot t) + cc \quad (6)$$

By defining two new variables, η and Δf, as

$$\eta = \nu_{QCL} - r \times f_{rep}^{fs}, \quad \text{with} \quad r = \text{int}(f_{rep}^{QCL}/f_{rep}^{fs}) \quad (7)$$

and

$$\Delta f = f_{rep}^{QCL} - k \times f_{rep}^{fs}, \quad \text{with} \quad k = \text{int}(f_{rep}^{QCL}/f_{rep}^{fs}) \quad (8)$$

we can re-express equation (6) as

$$\begin{aligned} E_s(t) &= \exp(i \cdot 2\pi\eta \cdot t) \times f_{rep}^{fs} \sum_{m=-q}^{m=+p} E_m \exp(i \cdot 2\pi m\Delta f \cdot t + \phi_m) \times \sum_{n=-\infty}^{n=+\infty} \exp[i \cdot (2\pi(r + m \cdot k + n) f_{rep}^{fs} \cdot t)] + cc \\ &= \exp(i \cdot 2\pi\eta \cdot t) \times f_{rep}^{fs} \sum_{m=-q}^{m=+p} E_m \exp(i \cdot 2\pi m\Delta f \cdot t + \phi_m) \times \sum_{n=-\infty}^{n=+\infty} \exp(i \cdot 2\pi n f_{rep}^{fs} \cdot t) + cc \\ &= \left[\exp(i \cdot 2\pi\eta \cdot t) \times \sum_{m=-q}^{m=+p} E_m \exp(i \cdot 2\pi m\Delta f \cdot t + \phi_m)\right] \times \sum_{n=-\infty}^{n=+\infty} \delta\left(t - \frac{n}{f_{rep}^{fs}}\right) + cc \end{aligned} \quad (9)$$

which leads to equation (4) in the main text.

Electro-optic detection. The terahertz QCL and femtosecond-laser beam were focused onto a 2-mm-thick (110) ZnTe electro-optic crystal. Both beams were linearly polarized along the [1,–1,0] axis. The terahertz field induced an a.c. birefringence, thus modulating the polarization state of the femtosecond-laser beam[42]. The crystal was followed by a quarter-wave plate to compensate the ZnTe static birefringence, so that the polarization of the femtosecond laser remained linear in the absence of terahertz radiation. After passing through a half-wave plate, the femtosecond laser was incident on a polarizing beamsplitter (PBS) rotated at 45° with respect to the axis of the half-wave plate. This transformed the polarization modulation driven by the terahertz a.c. field into an amplitude modulation; that is, the terahertz QCL electric field amplitude was sampled by the femtosecond laser (see equation (2))[29]. The two beams at the output of the PBS were detected with a balanced detection unit comprising two silicon photodiodes (Hamamatsu S3399) connected to a transimpedance amplifier, with a bandwidth of ~300 MHz (ref. 29).

Phase-locking of the longitudinal modes. Figure 6 shows the normalized spectra of the phase-locked line of Fig. 4c (L0) and of the five lines on its right (labelled L1, L2, . . . , L5) measured with a RBW of 1 Hz, the limit of our spectrum analyser (for clarity we subtracted the frequency offset of each line). As expected, from the ~25 dB amplitude measured at 100 kHz RBW (Fig. 4c), the amplitude of L0 increases to ~80 dB at 1 Hz, showing that the latter is well phase-locked to f_{rep}^{fs}. We also note that when moving away from L0, the phase noise increases from L1 to L5. This is also expected, because, contrary to L0, which is directly phase-locked, lines L1 to L5 are phase-locked to f_{rep}^{fs} only through the injection-locking process using RF-1. Now, RF-1 (and thus f_{rep}^{QCL}) presents a residual phase noise with respect to RF-2, due to the unavoidable excess noise present in any RF synthesis process. This residual phase noise results in the +20 dB (from –80 to –60 dBm) noise increment from L0 to L1, as shown in Fig. 6. As a consequence of the frequency multiplication process, we expect this phase noise to scale as the square of the line index for all the other lines. This is shown in the inset of the figure, where the phase-noise increment from L1, measured for each line at 30 Hz from the carrier frequency (black dots), is plotted as a function of the line index (n) on a log–log scale: within the error, the experimental points are in good agreement with the theoretical noise increment (red line), given by $(10 \times \log(n^2))$. This proves that when the QCL is injection-locked by RF-1 the phases ϕ_m of each longitudinal mode are constant.

Received 4 October 2010; accepted 21 February 2011; published online 24 April 2011; corrected online 26 April 2011

References

1. Paiella, R. (ed.) *Intersubband Transitions in Quantum Structures* (McGraw Hill Nanoscience and Technology, 2006).
2. Paiella, R. *et al.* High-frequency modulation without the relaxation oscillation resonance in quantum cascade lasers. *Appl. Phys. Lett.* **79,** 2526–2528 (2001).
3. Köhler, R. *et al.* Terahertz semiconductor–heterostructure laser. *Nature* **417,** 156–159 (2002).
4. Scalari, G. *et al.* THz and sub-THz quantum cascade lasers. *Laser Photon. Rev.* **3,** 45–66 (2009).
5. Williams, B. S. Terahertz quantum cascade lasers. *Nature Photon.* **1,** 517–525 (2007).
6. Kumar, S., Hu, Q. & Reno, J. 186 K operation of terahertz quantum-cascade lasers based on a diagonal design. *Appl. Phys. Lett.* **94,** 131105 (2009).
7. Barbieri, S. *et al.* 2.9 THz quantum cascade lasers operating up to 70 K in continuous wave. *Appl. Phys. Lett.* **85,** 1674–1676 (2004).
8. Barbieri, S. *et al.* 13 GHz direct modulation of terahertz quantum cascade lasers. *Appl. Phys. Lett.* **91,** 143510 (2007).
9. Maineult, W. *et al.* Microwave modulation of THz quantum cascade lasers: a transmission-line approach. *Appl. Phys. Lett.* **96,** 021108 (2010).
10. Wanke, M. C. *et al.* Monolithically integrated solid-state terahertz transceivers. *Nature Photon.* **4,** 565–569 (2010).
11. Gellie, P. *et al.* Injection-locking of terahertz quantum cascade lasers up to 35 GHz using RF amplitude modulation. *Opt. Express* **18,** 20799–20816 (2010).
12. Paiella, R. *et al.* Monolithic active mode-locking of quantum cascade lasers. *Appl. Phys. Lett.* **77,** 169–171 (2000).
13. Paiella, R. *et al.* Self mode-locking of quantum cascade lasers with giant ultrafast optical non-linearities. *Science* **290,** 1739–1742 (2000).
14. Wang, C. Y. *et al.* Coherent instabilities in a semiconductor laser with fast gain recovery. *Phys. Rev. A* **75,** 031802 (2007).
15. Choi, H. *et al.* Gain recovery dynamics and photon-driven transport in quantum cascade lasers. *Phys. Rev. Lett.* **100,** 167401 (2008).
16. Wang, C. Y. *et al.* Mode-locked pulses from mid-infrared quantum cascade lasers. *Opt. Express* **17,** 12929–12943 (2009).
17. Amanti, M. *et al.* Bound-to-continuum terahertz quantum cascade laser with a single-quantum-well phonon extraction/injection stage. *New J. Phys.* **11,** 1–19 (2009).
18. Walther, C., Scalari, G., Faist, J., Beere, H. & Ritchie, D. Low frequency terahertz quantum cascade laser operating from 1.6 to 1.8 THz. *Appl. Phys. Lett.* **89,** 231121 (2006).
19. Walther, C. *et al.* Quantum cascade laser operating from 1.2 to 1.6 THz. *Appl. Phys. Lett.* **91,** 131122 (2007).
20. Elzinga, P. A. *et al.* Pump/probe method for fast analysis of visible spectral signatures utilizing asynchronous optical sampling. *Appl. Opt.* **26,** 4303–4309 (1987).
21. Adachi, S., Takeyama, S. & Tagaki, Y. Dual wavelength optical sampling technique for ultrafast transient bleaching spectroscopy. *Opt. Commun.* **117,** 71–77 (1995).
22. Janke, C., Forst, M., Nagel, M., Kurz, H. & Bartels, A. Asynchronous optical sampling for high-speed characterisation of integrated resonant terahertz sensors. *Opt. Lett.* **11,** 1405–1407 (2005).
23. Yasui, T., Saneyoshi, E. & Araki, T. Asynchronous optical sampling terahertz time-domain spectroscopy for ultrahigh spectral resolution and rapid data acquisition. *Appl. Phys. Lett.* **87,** 061101 (2005).
24. Gebs, R., Klatt, G., Janke, C., Dekorsy, T. & Bartels, A. High-speed asynchronous optical sampling with sub-50 fs time resolution. *Opt. Express* **18,** 5974–5983 (2010).
25. Bartels, A. *et al.* Ultrafast time-domain spectroscopy based on high-speed asynchronous optical sampling. *Rev. Sci. Instrum.* **78,** 035107 (2007).
26. Shelton, R. K. *et al.* Phase-coherent optical pulse synthesis from separate femtosecond lasers. *Science* **17,** 1286–1289 (2001).
27. Coddington, I., Swann, W. C. & Newbury, N. R. Coherent multiheterodyne spectroscopy using stabilized optical frequency combs. *Phys. Rev. Lett.* **100,** 013902 (2008).
28. Schliesser, A., Brehm, M., Keilmann, F. & Weide, D. W. Frequency-comb infrared spectrometer for rapid, remote chemical sensing. *Opt. Express* **13,** 9029–9038 (2005).
29. Barbieri, S. *et al.* Phase-locking of a 2.7 THz quantum cascade laser to a mode-locked erbium-doped fibre laser. *Nature Photon.* **4,** 636–640 (2010).
30. Udem, Th., Holzwarth, R. & Hansch, T. Optical frequency metrology. *Nature* **416,** 233–237 (2002).
31. Jones, D. J. *et al.* Carrier-envelope phase control of femtosecond mode-locked lasers and direct optical frequency synthesis. *Science* **288,** 635–699 (2000).
32. Barbieri, S. *et al.* Heterodyne mixing of two far-infrared quantum cascade lasers by use of a point-contact Schottky diode. *Opt. Lett.* **29,** 1632–1634 (2004).
33. Barkan, A. *et al.* Linewidth and tuning characteristics of terahertz quantum cascade lasers. *Opt. Lett.* **29,** 575–577 (2004).

34. Hensley, J. M. *et al.* Spectral behaviour of a terahertz quantum cascade laser. *Opt. Express* **17,** 20476–20483 (2009).
35. McDuff, O. P. & Harris, S. E. Nonlinear theory of internally loss-modulated laser. *IEEE J. Quantum Electron.* **3,** 101–111 (1967).
36. Kroll, J. *et al.* Phase-resolved measurements of stimulated emission in a laser. *Nature* **449,** 698–701 (2007).
37. Jukam, N. *et al.* Investigation of spectral gain narrowing in quantum cascade lasers using terahertz time domain spectroscopy. *Appl. Phys. Lett.* **93,** 101115 (2008).
38. Jukam, N. *et al.* Terahertz time domain spectroscopy of phonon-depopulation based quantum cascade lasers. *Appl. Phys. Lett.* **94,** 251108 (2009).
39. Gordon, A. *et al.* Multimode regimes in quantum cascade lasers: from coherent instabilities to spatial hole burning. *Phys. Rev. A* **77,** 053804 (2008).
40. Gkortsas, V.-M. *et al.* Dynamics of actively mode-locked quantum cascade lasers. *Opt. Express* **18,** 13616–13630 (2010).
41. Scalari, G. *et al.* Broadband THz lasing from a photon–phonon quantum cascade structure. *Opt. Express* **18,** 8043–8052 (2010).
42. Sakai, K. (ed.) *Terahertz Optoelectronics* (Springer, 2005).

Acknowledgements

The authors thank R. Barbieri for carefully checking the sampling formulae. Partial financial support was received from the Délégation Générale pour l'Armement (contract no. 06.34.020), the ANR agency (contract HI-TEQ), the EPSRC (UK) and the European Research Council programmes 'NOTES' and 'TOSCA'. Device fabrication was performed at the CTU-IEF-Minerve, which is partially funded by the Conseil Général de l'Essonne.

Author contributions

S.B. conceived and performed the experiment, analysed data and wrote the paper. M.R. performed the experiment, analysed data and contributed to manuscript preparation. P.G. performed the experiment and analysed the data. G.S. conceived and performed the experiment, analysed data and contributed to manuscript preparation. C.M. fabricated the quantum cascade laser. C.S. analysed the data and contributed to manuscript preparation. S.P.K. grew the quantum cascade laser material used for this work, under the supervision of E.H.L. and A.G.D.

Additional information

The authors declare no competing financial interests. Reprints and permission information is available online at http://www.nature.com/reprints/. Correspondence and requests for materials should be addressed to S.B.